



Improving Force Measurements in Ludwieg Tunnels

Jack Hillyer ¹, Luke Doherty ¹, Matthew McGilvray ¹

Abstract

This paper presents experimental results from testing aimed to improve force balance measurements in Ludwieg tunnels. This is achieved by leveraging the extended rise time and test duration of the recently commissioned Extended Ludwieg Mode to 1) investigate the effect of nozzle supply pressure rise time on model/force balance natural frequency excitation and 2) assess the suitability of a 6 Degree of Freedom Inertial Measurement Unit for acceleration compensation. It is demonstrated that for Ludwieg Tunnels, addition of a plenum between the fast acting valve and the nozzle throat can reduce the magnitude of the startup loads - typically an order of magnitude greater than the test loads - and consequently enables use of a balance with a lower full scale range and associated lower uncertainties. Furthermore, it is also shown that the duration of the nozzle startup period, not the overall rise time of the facility nozzle supply trace, dictates which model-balance natural frequencies are excited. Finally, it is demonstrated that a 6 Degree of Freedom Inertial Measurement Unit can be used for acceleration compensation, including use of differentiated gyroscope measurements for moment compensation, potentially alleviating some packaging constraints for accelerometer placement inside the model.

Keywords: hypersonic, acceleration compensation, MEMS IMU

Nomenclature

Latin

a – Acceleration C – Coefficient

D – Drag

FB – Force Balance

L - Rolling moment M - Mach Number

q – Dynamic Pressure

q - Dynamic Fressure

Greek

 α – Angle of attack

 β – Angle of sideslip

 δ – Control effector deflection

 ϕ – Roll angle

Subscripts

AC - Acceleration compensated

I - Rolling

UC - Uncompensated

1. Introduction

In any speed regime, the backbone of flight vehicle design is the generation of a high quality aerodynamic database in the form of aerodynamic coefficients. Values for these coefficients can be numerically predicted using Computational Fluid Dynamics (CFD) [1-4], experimentally measured in ground test facilities [5-7], or generated from flight data [8-10], with the trend moving towards numerical techniques as their physical fidelity has grown. However, CFD still requires validation data to improve confidence in its predictions and consequently wind tunnel testing still plays an important role in flight vehicle design.

Hypersonics is currently undergoing a resurgence of interest for both civil and military applications. As a result of the high energies involved in generating these flows, hypersonic facilities are often of impulse nature. A common type of hypersonic ground test facility, owing to their low cost and simple operation, is the Ludwieg Tunnel. These are low enthalpy facilities, unable to replicate high temperature gas effects but able to match flight Mach and Reynolds number, thereby proving extremely useful for investigation of aerodynamic phenomena.

¹University of Oxford, corresponding email address: jack.hillyer@eng.ox.ac.uk

Force measurements in Ludwieg tunnels are complicated by their impulsive nature (specifically, high startup forces, rapid flow initialisation and short test durations) inducing vibrations in the force measurement system that superpose on the measured force signal. It is expected that an increase in rise time of the facility nozzle supply pressure trace will excite fewer of the force measurement system's natural frequencies and consequently reduce the magnitude of these vibrations [11]. Where this is not possible, custom force balances (designed for maximum natural frequency) [12–14], and acceleration compensation [15-19] can be used to minimise/remove the oscillatory content. To date, acceleration compensation has exclusively used linear accelerometers, with their location in the model being a compromise of geometry and signal quality - accelerometers compensating force measurements are ideally situated as close as possible to the force balance to maximise the likelihood the measured accelerations are in phase with the force measurement, whilst accelerometers compensating moments are ideally placed at model extremities to maximise signal. Use of a 6 Degree-of-Freedom (6-DoF) Micro Electrical Mechanical Systems (MEMS) Inertial Measurement Unit (IMU), such as those those typically used in freeflight experiments [20-25], may allow for fewer compromises in accelerometer placement, but these are yet to be demonstrated as suitable for acceleration compensation in impulse facilities - particularly for moment compensation where angular accelerations are attained from differentiation of gyroscope measurements.

This paper leverages the extended test time capability of the recently implemented Extended Ludwieg Mode (ELM) [26, 27] to improve force balance measurements in Ludwieg tunnels. Firstly, the effect of the extended rise time and test duration of ELM relative to standard Ludwieg Tunnel operation on the oscillatory content in the measured force traces is explored, and the suitability of a 6-DoF MEMS IMU for acceleration compensation is investigated. The experimental model is a 10 degree half-angle cone fitted with all moving wings, and the primary measurements are of drag and rolling moment.

The remainder of this paper is organised as follows: descriptions of the experimental facility and model are given in Section 2 and Section 3, respectively. The data reduction techniques are explained in Section 4, and experimental results are presented in Section 5. Finally, conclusions are presented in Section 6.

2. Facility

2.1. The Oxford High Density Tunnel

All tests in this paper were performed in the Oxford High Density Tunnel (HDT), a Ludwieg tunnel located at the Oxford Thermofluids Institute, University of Oxford [28]. A schematic of the facility is given in Fig. 1, featuring a barrel of internal diameter 152 mm and length 17.35 m. The barrel is separated from the nozzle plenum by an upstream facing plug valve. The HDT features four operational nozzles, each with an exit diameter of 351 mm, covering the range of Mach 4 to Mach 7. The facility barrel can be heated to 550 K, and has a maximum pressure rating of 275 bar.

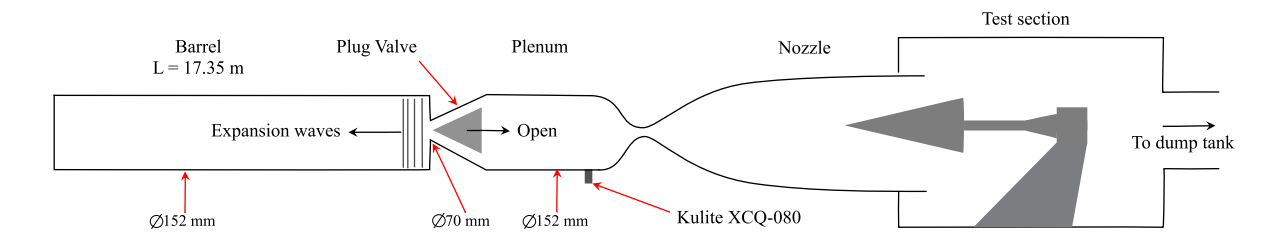


Fig 1. Schematic of HDT. Adapted from [29]

The HDT is currently capable of being operated in 4 modes: 1) Ludwieg Mode (LM), 2) Light Isentropic Compression Heating (LICH), 3) Extended Ludwieg Mode (ELM) and 4) Plenum Augmented Ludwieg Mode (PALM). ELM and PALM are proposed as the most suitable of these modes for force balance experiments owing to their increased test duration, allowing more time for vibrations to damp out, and

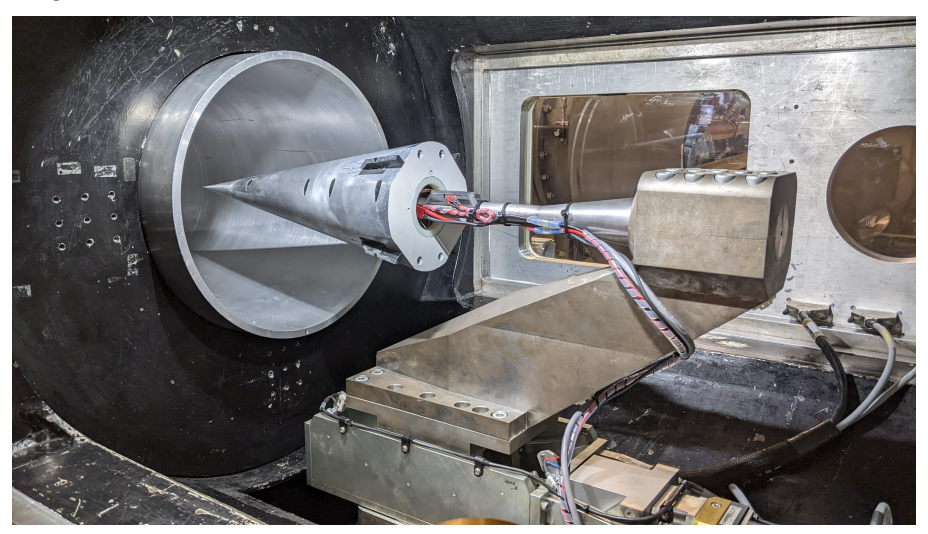
extended rise time, slightly relaxing the requirement for high natural frequency of the force balance system. Unfortunately PALM was still under active development during these experiments so was not available to be used. The majority of tests presented in this paper were performed in ELM, though LM was also used to investigate the effect of supply pressure rise time on the form of the measured force trace.

2.2. Instrumentation

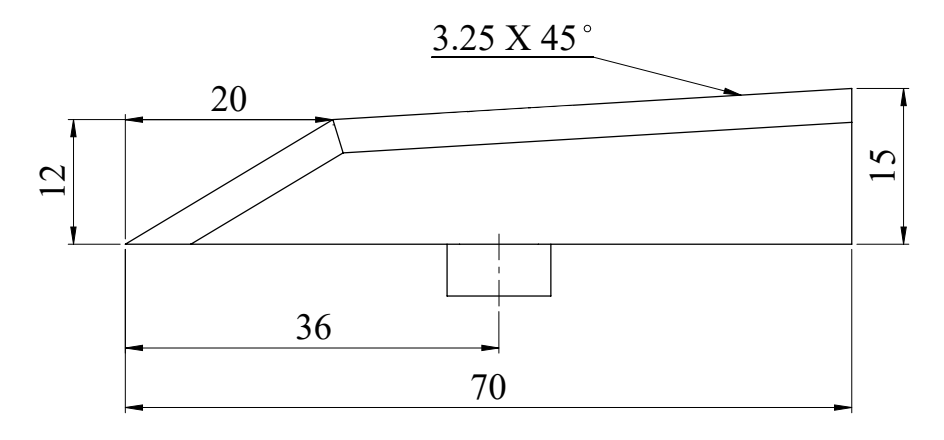
Nozzle supply conditions were measured using sensors mounted in the facility plenum. The supply pressure was measured using a flush mounted Kulite XCQ-080 transducer, and total temperature calculated from Aspirated Thermocouple (ATC) data using the processing outlined in [29,30]. The Kulite was amplified with a Fylde FE-H379-TA differential amplifier, and the ATC with an Adafruit AD8495 amplifier. Both supply condition sensors were recorded at 100 kHz on NI PXIE 6368 cards housed in a NI PXIe-1092 chassis (henceforth referred to as the NI DAQ).

3. Experimental Model

3.1. Geometry



(a) Installed in the test section on the two axis traverse in force balance configuration



(b) All moving wing geometry. All dimensions in millimetres

Fig 2. Experimental model

The experimental model used in this campaign, shown installed in the test section in Fig. 2a, consisted of a 10 degree half angle cone with base diameter 148.5mm, fitted with 4 all-moving wings in an X

Table 1. Summary of model properties. Inertia is the inertia about the cone axis. Inertia and Centre of Gravity (CoG) measured using a raptor scientific KSR330.

Property	Unit	Value	Uncertainty		
Nose radius	mm	1.25	-		
Half angle	0	10	-		
Base diameter	mm	148.5	± 0.2		
S_{ref}	m^2	0.0173	± 0.0001		
Mass	kg	3.5	± 0.1		
Inertia, J	${\sf kg}{\sf m}^2$	0.0068	$\pm 8.5\times 10^{-5}$		
CoG (radius)	mm	0.18	± 0.2		

configuration. To reduce root gap effects, the wings were situated on flats machined into the cone surface. These flats themselves are 3 degree expansions relative to the cone surface, chosen to give sufficient space for the full range of wing motion whilst minimising the static pressure decrease through the expansion. All cone components were manufactured from Aluminium 7075 T6, and a summary of the model properties is given in Table 1, where the moment of inertia was measured with a Raptor Scientific KSR 330.

The wings are 3D printed and positioned by DFRobot SER0044 servo motors, driven with a BK Precision 1688B power supply. The wing geometry is shown in Fig. 2b, and can be seen to have a length of 70 mm and a pivot at 51.5% chord.

A two axis traverse was used in these experiments for positioning the model in pitch and yaw. The traverse has a usable motion range of ± 15 degrees in pitch and ± 5 degrees in yaw, but is not able to be moved during the test.

3.2. Onboard Data Acquisition

The experimental model featured two onboard Data Acquisition Systems (DAQs): a "pressure" DAQ and a "control" DAQ, both triggered by the NI DAQ. Each onboard DAQ recorded a 6-axis TDK ICM-42688-P Inertial Measurement Unit (IMU) at 32 kHz, situated on satellite boards to decouple IMU placement from main DAQ board location. A summary of the IMU full scale range and associated uncertainties are given in Table 2. The IMU connected to the control DAQ was mounted on the sting while the IMU recorded by the pressure DAQ was mounted in the model on the centreline, just upstream of the force balance. The pressure DAQ recorded a further 4 Honeywell HSCMAND015PASA5 pressure transducers at 4 kHz, recess mounted on the cone flats (approximately 14 mm upstream of wing tips), and used for model alignment, whilst the control DAQ changed wing servo position between tests and recorded their feedback position.

Table 2. TDK ICM-42688-P IMU full scale range and uncertainties. All taken from manufacturers datasheet

Sensor	Full Scale Range	Uncertainty		
Gyroscopes	$\pm 2000{}^{\circ}\mathrm{S}^{-1}$	$\pm 2~^{\circ}\mathrm{S}^{-1}$		
Accelerometers	$\pm 16g$	$\pm 0.016g$		

3.3. Force Balance

The force balance used in these experiments was an ATI-Mini45, calibration type SI-145-5. A summary of its load ratings and natural frequencies are given in Table 3. The force balance has three sensing beams, with applied loads being measured by silicon semiconductor strain gauges arranged in six half-

bridge pairs. Simple bridge completion circuity, mounted in the test section, was used so the force balance could be amplified by a Fylde FE-H379-TA differential amplifier and recorded on the NI DAQ at 100 kHz. The manufacturer provided static calibration was used after verification of its accuracy with an in-house static calibration. This force balance was acceleration compensated using the IMU's recorded by the two onboard DAQs.

Table 3. ATI Mini 45 specifications. Note that the natural frequencies listed are for the force balance in isolation. When installed in the model, the additional mass reduces the overall natural frequency of the system [12, 16].

Axis	Full Scale Range	Uncertainty	Natural Frequency		
Drag	290 N	\pm 2.175 N	5.4 kHz		
Rolling Moment	5 N m	\pm 0.0625 N m	5.6 kHz		

4. Data Reduction

This section presents an explanation of the data reduction used in this paper, detailing the calculation of freestream properties and acceleration compensation.

4.1. Freestream Conditions

Freestream conditions were calculated assuming isentropic expansion of calorifically perfect air from measured nozzle supply pressure and calculated total temperature data. Total temperature was calculated from plenum based ATC measurements using the processing in [29, 30]. Mach number was assumed to be constant across the test, with the value taken from the measured centreline Mach Number from a Pitot rake shot at the chosen fill conditions. Viscosity was calculated using Keyes relation [31]. Uncertainties, given in Table 4, were propagated through the data reduction equations using the jitter methodology (5 point stencil and a 0.2% perturbation magnitude) [32].

Table 4. Summary of the input uncertainties to the supply condition calculations

Class Dramarks	DO.	Τ0	M		
Flow Property	Р0	ТО	LM	ELM	
Sensor	Kulite XCQ-80	ATC	Assumed Constant		
Value	Measured	Measured	7.04	7.00	
Uncertainty	\pm 7000 Pa (0.1% FSO)	$\pm 15~\text{K}$	± 0.06	± 0.071	

4.2. Acceleration Compensated Force Balance

Though the Mini45 is a 6 axis force balance, only the drag and rolling moment measurements are presented in this work. Hence, this section presents an outline of the data reduction used for compensation of those signals, though naturally these processes can be extended to other axes with appropriate axes transformations and filter widths. As the force balance and the IMU were recorded at different sample rates (100 and 32 kHz, respectively), some resampling was necessary. In this work, it was chosen to downsample both traces onto a common timebase to avoid interpolation of data points complicating the uncertainty calculations. The final point to be addressed before moving onto the explanation of the data reduction is the time alignment of the IMU and force balance data (recorded on different DAQs). This was achieved with a least-squares optimisation process, whereby the drag/rolling moment coefficient was assumed constant for a chosen test window (i.e. drag/rolling moment directly follows supply pressure trace) and time alignment shifted to minimise the deviations of the resultant acceleration compensated measurement from a straight line of best fit through the unfiltered/oscillatory data. This process is not dissimilar to the processed used in Störkmann [16], though in that case the least-squares fit was used in determination of the C_{AC} matrix discussed later.

The underlying equations for acceleration compensation of the drag and rolling moment are given in Eq. 1 and Eq 2, respectively:

$$D_{AC} = D_{UC} - C_{AC} * a_x$$
 (1) $L_{AC} = L_{UC} - C_{AC} * \ddot{\phi}$

Where D_{AC} and L_{AC} are the acceleration compensated drag and rolling moment, respectively, D_{UC} and L_{UC} are the uncompensated drag and rolling moment, respectively, C_{AC} is a calibration matrix relating the inertial forces to accelerometer readings, a_x is the acceleration in the body x-axis and $\ddot{\phi}$ is the angular acceleration about the cone axis.

The process for acceleration compensation of the drag is as follows:

- 1. Transform IMU axes into body axes
- 2. Convert from g's to $m s^{-2}$, assuming 9.81 $m s^{-2}$ for local gravity.
- 3. Set the initial pre-test accelerations to zero to remove contributions from gravity.
- 4. Downsample all force and acceleration data onto a common timebase (4 kHz).
- 5. Perform the acceleration compensation as per Eq 1, with C_{AC} equal to the mass of the model

For the rolling moment, the angular acceleration is attained from differentiation of the gyroscope readings as follows:

- 1. Transform IMU axes into body axes
- 2. Convert from $^{\circ}$ s $^{-1}$ to rad s $^{-1}$
- 3. Pre-smooth the angular rates with a 3ms moving average filter.
- 4. Downsample all force and angular rate data onto a common timebase (4 kHz).
- 5. Differentiate angular rates to attain angular accelerations.
- 6. Smooth angular acceleration data with a 2.5ms moving average filter.
- 7. Perform the acceleration compensation as per Eq 2, with C_{AC} equal to the inertia of the model about the cone axis.

The overall rolling moment measured by the force balance is then given by Eq. 3:

$$L_{AC} = L_{aero} + L_{CoG} + L_{offset} \tag{3}$$

Where L_{CoG} is the rolling moment arising from displacement between the force balance sensing origin and the model centre of gravity, and L_{offset} is a reported rolling moment arising from zero bias of the strain gauges. If the force balance is zeroed prior to the test, the output, L_{AC} , then reduces to L_{nero} .

5. Experimental Results

5.1. Facility Nozzle Supply Conditions

All tests in this paper were performed at Mach 7 with fill conditions of 8 bar and 500 K, corresponding to an 38km altitude flight condition at one to five scale. Typical supply condition traces of the HDT operating in LM and ELM are shown in Fig. 3, with LM producing several steady flow plateaus of 35 ms duration and ELM demonstrating an increased rise time followed by a steady decrease in supply pressure for approximately 400 ms. A detailed explanation of the form of each trace is given in [26].

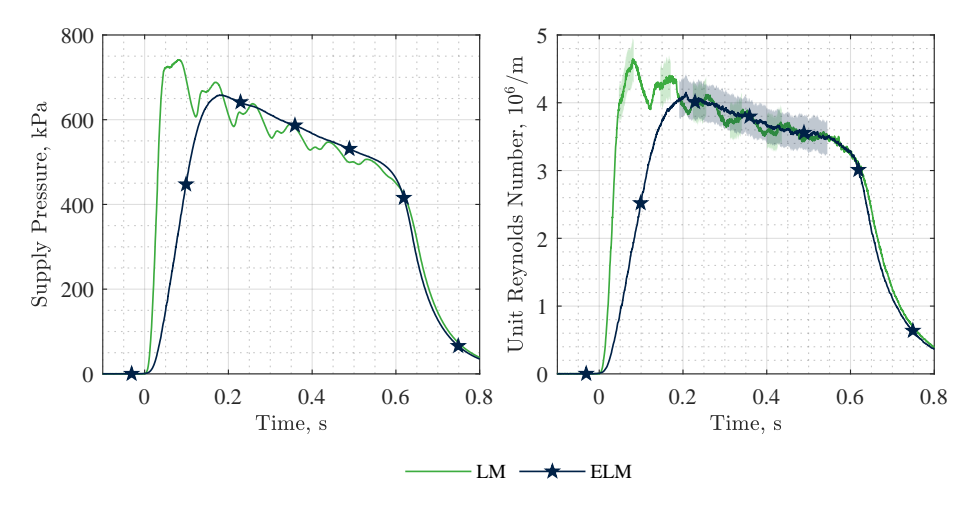


Fig 3. HDT Nozzle supply conditions used in these experiments. Uncertainties are present on the supply pressure plot, but are too small to see

5.2. Effect of Rise Time/Nozzle Startup and Test Duration

Fig. 4a and Fig 4b present the unfiltered drag and rolling moment, respectively, attained from shots operated in LM and ELM to investigate the effect of rise time and test duration on resultant force measurements. It can be seen that all traces broadly follow their respective supply pressure traces (cf. Fig. 3), but feature transient spikes and oscillations as a consequence of excitation of the model-balance system natural frequencies. There are two natural frequencies of importance for the Drag measurements: 1) the natural frequency of the sting ($\approx 35~\text{Hz}$) and 2) the natural frequency of the force balance and the model itself ($\approx 500~\text{Hz}$). For the rolling moment, the response is only dominated by the natural frequency of the model and force balance ($\approx 100~\text{Hz}$). It can be seen that the quality of the drag measurements is comparable in each operating mode, though the LM trace demonstrates excitation of the 500 Hz mode on each plateau. In comparison, for the rolling moment, it can be seen that operation in ELM results in a significant increase in oscillation magnitude despite the increased rise time - contrary to expectations given existing literature [11, 13].

The Pitot pressure traces shown in Fig. 5, taken from a 14 bar shot in each mode, reveal the cause of the increased oscillation magnitude in ELM. Two shocks arising from the nozzle starting process can be seen for both modes, with ELM producing shocks that are both stronger and further apart in time. Defining the nozzle startup time as from when the pressure starts to rise to the passage of the second shock, it can be seen that this is approximately 5 ms for the LM case, whilst for ELM it is approximately 12 ms. The characteristic times of the system are summarised in Table 5, demonstrating the increased oscillation magnitude of the rolling moment in ELM is a consequence of the increased duration of the nozzle startup period. Hence, it is the duration of the nozzle startup period, as opposed to the overall rise time of the supply pressure, that is important for excitation of the natural frequencies of the system. However, as expected, the extended test duration available in ELM allows for the induced vibrations to damp out, ultimately culminating in lower oscillation magnitudes at the end of the test.

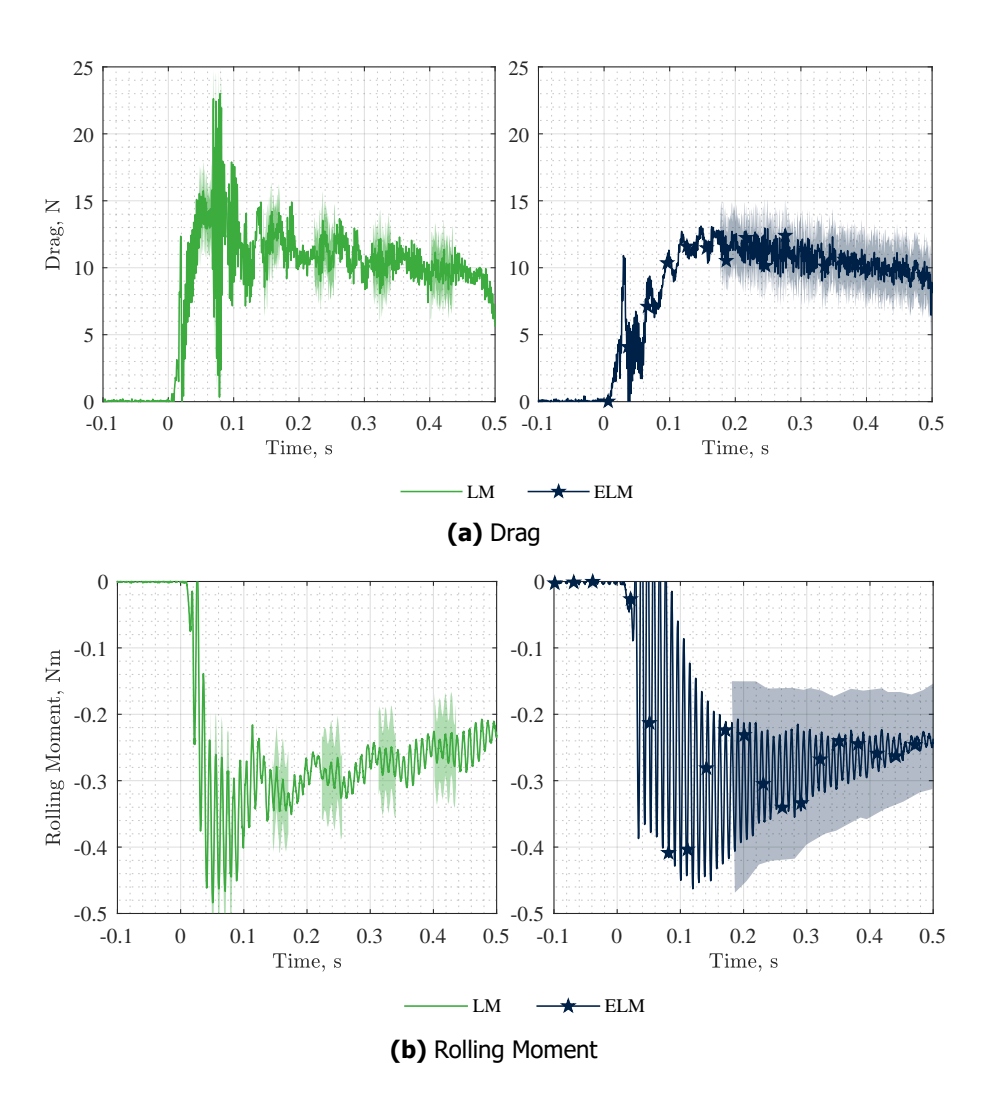


Fig 4. Uncompensated, unfiltered force measurements in LM (left) and ELM (right).

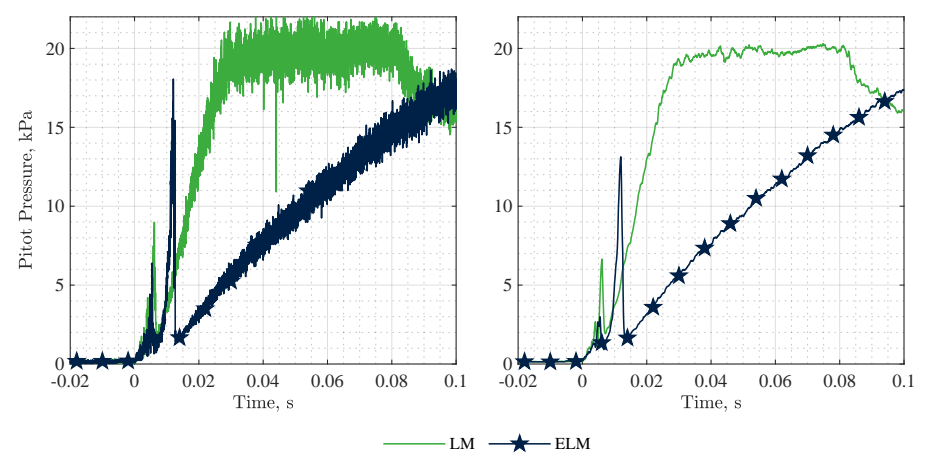


Fig 5. Unfiltered (left) and 1kHz low pass filtered (right) Pitot Pressure traces in LM (shot 3614) and ELM (shot 3623). For both traces, t=0 is set to flow arrival

Table 5. Summary of characteristic times of the force balance and supply pressures, Nozzle startup is defined as the time between the pitot pressure starting to rise and the passing of the secondary nozzle shock. FB = Force Balance

	Drag		Rolling Moment	Rise Time		Nozzle Startup	
	Sting	FB	FB	LM	ELM	LM	ELM
Characteristic Time, ms	28	2	10	25	110	5	12

It should be noted that whilst both Fig. 4a and Fig 4b show a transient increase in drag and rolling moment near the start of the test in both modes (occurring at $t=20 \mathrm{ms}$ for LM and at $t=30 \mathrm{ms}$ for ELM), the magnitude of this increase is less than the peak value measured during the test - atypical of force measurements in impulse facilities. This is a consequence of the HDT featuring a plenum between the barrel and nozzle throat, allowing the nozzle starting process to occur at a lower supply pressure and reducing the strength of the starting shocks. This observation allows future experimenters to size their force balance load rating based on the forces expected during the test as opposed to the startup forces, reducing uncertainty in the measurements.

5.3. Acceleration Compensation

This section presents results from acceleration compensation of the force balance data. Noting that acceleration compensation serves only to reduce the oscillations about the mean value, rather than affecting the mean value itself, the presented uncertainties are those provided by the force balance manufacturer (cf. Table 3).

Fig. 6b and Fig. 6c present model and sting based acceleration compensation, respectively, of the drag in both modes. It can be seen that neither compensation technique is able to significantly improve the quality of the drag measurements in LM, though model based compensation does reduce the magnitude of the transient variation for $0.07 \le t \le 0.1$ s. The relative advantages of each acceleration compensation technique are well demonstrated by the ELM data in Fig. 6b and Fig. 6c, where it can be seen that model based compensation is able to remove the majority of the contributions from force balance natural frequencies, whereas the sting based acceleration compensation is able to remove the lower frequency oscillations attributed to the sting vibrations.

Noting that this paper presents the first time 1 that acceleration compensation of a moment measurement has been performed using differentiated gyroscope data from a 6 DoF MEMS IMU, it is felt necessary to present the IMU data at the critical stages of data processing before presenting the acceleration compensated data itself. This is shown in Fig. 7, with gyroscope data being given in Fig. 7a and differentiated gyroscope data in Fig. 7b. As expected, the raw gyroscope data demonstrates clear oscillations about zero rad s $^{-1}$, at a frequency of approximately 500 Hz (force balance natural frequency). The moving average filter removes the transient oscillations superposed on this signal, though this comes at the cost of a slight reduction in the peak values of the trace. These trends are then repeated in the differentiated gyroscope data, though the magnitude of the transient oscillations superposed on the 500 Hz content is significantly reduced.

Fig. 8b presents acceleration compensation of the rolling moment in LM and ELM, demonstrating an almost complete reduction of the low frequency oscillations and significantly improving the quality of the data. Together, Fig. 6c, Fig. 7 and Fig. 8b demonstrate 6 axis MEMS IMU's are suitable for acceleration compensation in hypersonic Ludwieg tunnels, including the use of differentiated gyroscope measurements for moment compensation.

Overall, this section has demonstrated that the use of acceleration compensation in Ludwieg tunnels can significantly improve the quality of force and moment data attained (even without a custom force

¹To the authors knowledge

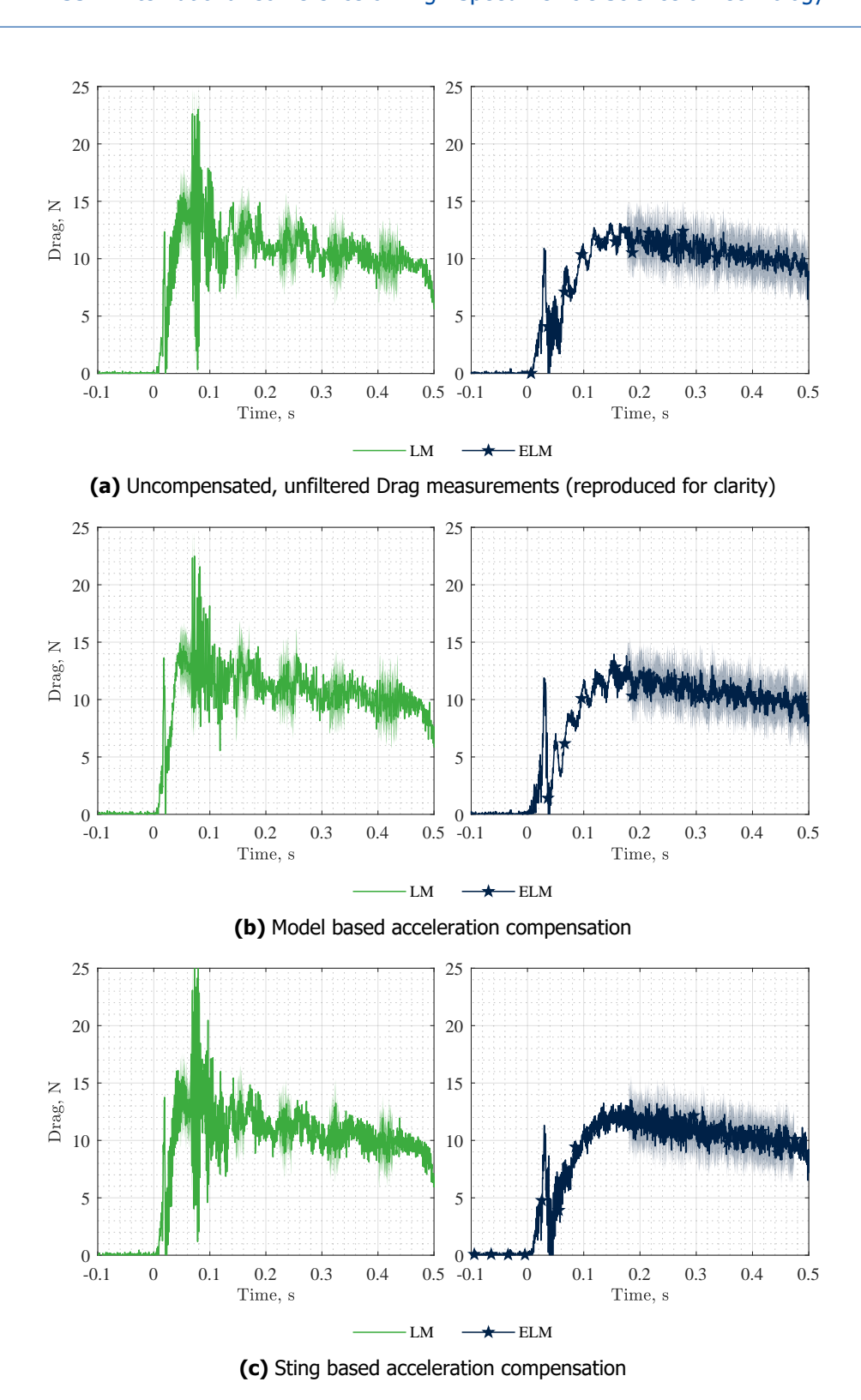
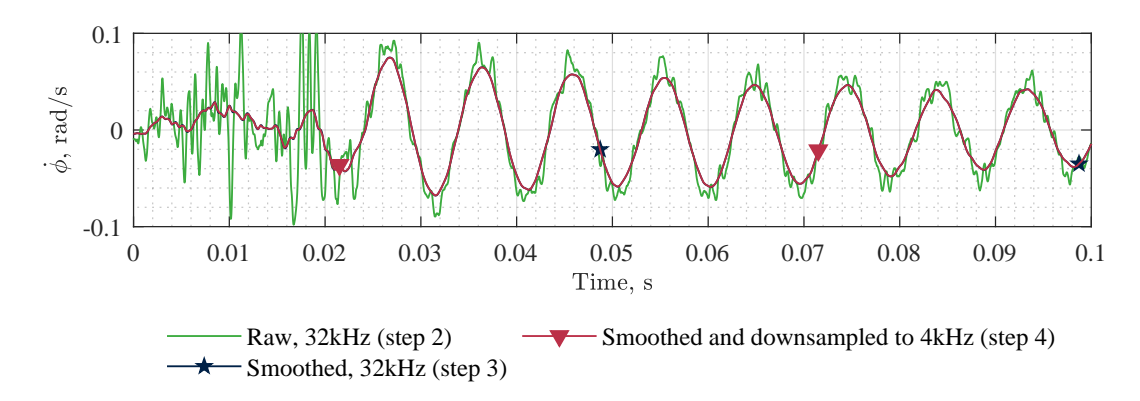
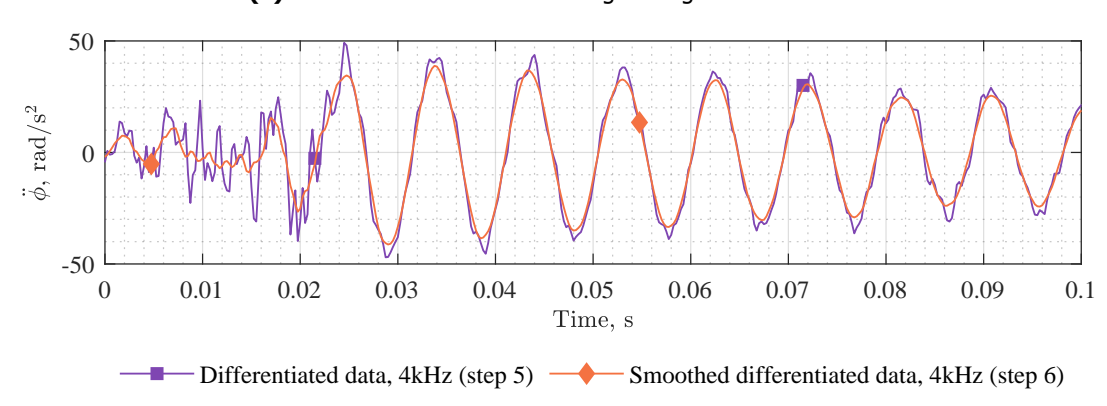


Fig 6. Acceleration compensated Drag measurements in LM (shot 3658, left) and ELM (shot 3653, right). For all traces, t=0 is set to flow arrival



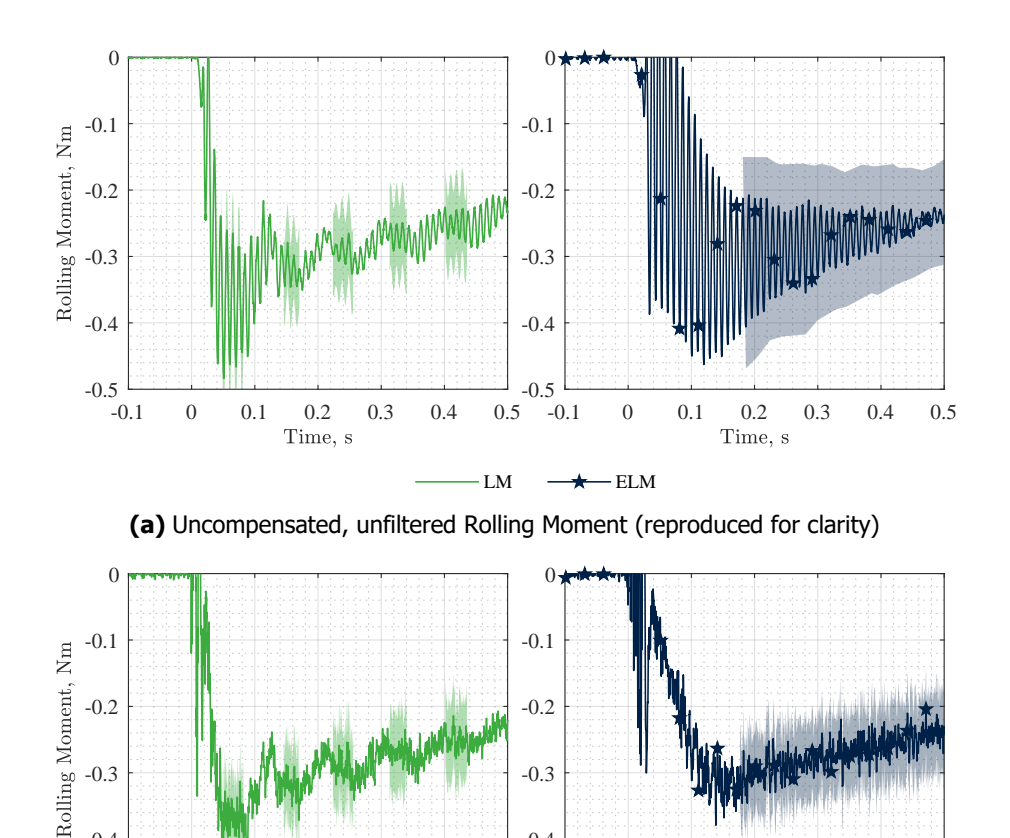
(a) Raw roll rate and 3 ms moving average filtered roll rate



(b) Angular acceleration, with and without a 2.5 ms moving average filter applied after differentiation

Fig 7. Data from the model IMU used in rolling moment compensation in ELM (shot 3653). Zoomed in relative to the plots to demonstrate the effect of filtering on the signal during processing

balance) and hence acceleration compensation is recommended for any force balance testing in facilities with similar test durations where commercial-off-the-shelf force balances are used.



LM (b) Model based acceleration compensation

0.5

0.3

0.2

Time, s

0.4

-0.3

-0.4

-0.5

-0.1

0.1

- ELM

0.2

Time, s

0.3

Fig 8. Rolling moment measurements in LM (shot 3658, left) and ELM (shot 3653, right). All data downsampled to 4 kHz as per processing outlined in Section 4.2.

6. Conclusion

-0.3

-0.4

-0.5

-0.1

0

This paper has presented experimental results from a campaign leveraging the extended test duration of the recently developed Extended Ludwieg Mode (ELM) to improve force balance measurements in hypersonic Ludwieg tunnels. It is demonstrated that for Ludwieg tunnels, it is the duration of nozzle startup period, not the overall rise time of the supply condition traces that serves to excite the natural frequencies of a force measurement system. It is also shown that addition of a plenum between the fast acting valve and the nozzle throat can reduce the magnitude of the startup loads imposed on the force balance. Noting that these are often an order of magnitude greater than the test loads, addition of a plenum to the Ludwieg Tunnel allows for lower full scale range force balances to be used, reducing the uncertainty. Finally, it is demonstrated that 6 axis MEMS IMU's are suitable for acceleration compensation in hypersonic Ludwieg tunnels, including use of differentiated gyroscope measurements for moment compensation.

7. Acknowledgements

This research was funded by DSTL. The authors would like to thank Mr Christopher Hambidge for his operation of HDT during this campaign.

0.5

0.4

References

- [1] Giuseppe Pezzella, Marco Marini, Marco Cicala, Antonio Vitale, Tobias Langener, and Johan Steelant. Aerodynamic characterization of hexafly scramjet propelled hypersonic vehicle. In 32nd AIAA Applied Aerodynamics Conference, page 2844, 2014.
- [2] Antonio Schettino, Giuseppe Pezzella, Marco Marini, Sara Di Benedetto, Victor F Villace, Johan Steelant, Rishabh Choudhury, Anatoly Gubanov, and Nina Voevodenko. Aerodynamic database of the hexafly-int hypersonic glider. *CEAS Space Journal*, 12:295–311, 2020.
- [3] Charles E Cockrell Jr, Aaron H Auslender, Jeffrey A White, and Arthur D Dilley. Aeroheating predictions for the x-43 cowl-closed configuration at mach 7 and 10. In 40th AIAA Aerospace Sciences Conference and Exhibit, number AIAA Paper 2002-0218, 2002.
- [4] Charles Cockrell, Jr, Walter Engelund, Arthur Dilley, Robert Bittner, Tom Jentink, and Abdelkader Frendi. Integrated aero-propulsive cfd methodology for the hyper-x flight experiment. In *18th Applied Aerodynamics Conference*, page 4010, 2000.
- [5] Scott D Holland, William C Woods, and Walter C Engelund. Hyper-x research vehicle experimental aerodynamics test program overview. *Journal of spacecraft and rockets*, 38(6):828–835, 2001.
- [6] Kelly J Murphy, Robert J Nowak, Richard A Thompson, Brian R Hollis, and Ramadas Prabhu. X-33 hypersonic aerodynamic characteristics. *Journal of Spacecraft and Rockets*, 38(5):670–683, 2001.
- [7] Patrick Gruhn and Ali Gülhan. Aerodynamic measurements of an air-breathing hypersonic vehicle at mach 3.5 to 8. *AIAA Journal*, 56(11):4282–4296, 2018.
- [8] Eugene A Morelli. Flight-test experiment design for characterizing stability and control of hypersonic vehicles. *Journal of Guidance, Control, and Dynamics*, 32(3):949–959, 2009.
- [9] Eugene A Morelli. Flight test maneuvers for efficient aerodynamic modeling. *Journal of aircraft*, 49(6):1857–1867, 2012.
- [10] Eugene Morelli, Stephen Derry, and Mark Smith. Aerodynamic parameter estimation for the x-43a (hyper-x) from flight data. In *AIAA atmospheric flight mechanics conference and exhibit*, page 5921, 2005.
- [11] Leonard Bernstein and Ronald Charles Pankhurst. Force measurements in short duration hypersonic facilities. 1975.
- [12] C Jessen and H Grönig. A six component balance for short duration hypersonic facilities. In *New trends in Instrumentation for hypersonic research*, pages 295–305. Springer, 1993.
- [13] Daniel Simmons, William D Gothard, Nicholas J Molinaro, and Ryan J Meritt. Wind tunnel balance development for ludwieg tube facilities. In *AIAA AVIATION FORUM AND ASCEND 2024*, page 4285, 2024.
- [14] Hideyuki Tanno, Katsuhiro Itoh, Tomoyuki Komuro, Kazuo Sato, and Syuichi Ueda. Design and evaluation of strain gauge force balance with short test duration. *Transactions of the Japan Society for Aeronautical and Space Sciences*, 48(159):1–6, 2005.
- [15] James F Martin and Leroy M Stevenson. *Instrumentation for force and pressure measurements in a hypersonic shock tunnel*. Number 113. Cornell Aeronautical Laboratory, Incorporated, 1962.
- [16] V Storkmann, H Olivier, and H Gronig. Force measurements in hypersonic impulse facilities. *AIAA journal*, 36(3):342–348, 1998.
- [17] Eric C Marineau. Force measurements in hypervelocity flows with an acceleration compensated piezoelectric balance. *Journal of spacecraft and rockets*, 48(4):697–700, 2011.
- [18] Eric C Marineau, Matthew MacLean, Erik P Mundy, and Michael S Holden. Force measurements in hypervelocity flows with an acceleration compensated strain gage balance. *Journal of Spacecraft and Rockets*, 49(3):474–482, 2012.

- [19] John W Draper, Greg Brauckmann, Franklin D Turbeville, and Sung Lee. Dynamic force reconstruction of transient flap control force experiments in a hypersonic wind tunnel. In *AIAA SCITECH* 2024 Forum, page 2661, 2024.
- [20] Andrew Hyslop, Luke J Doherty, Matthew McGilvray, Andrew Neely, Liam P McQuellin, James Barth, and Gerrie Mullen. Free-flight aerodynamic testing of the skylon space plane. *Journal of Spacecraft and Rockets*, 58(5):1487–1497, 2021.
- [21] Andrew M Hyslop, Matthew McGilvray, and Luke J Doherty. Free-flight aerodynamic testing of a 7 degree half-angle cone. In *AIAA SCITECH 2022 Forum*, page 1324, 2022.
- [22] AM Hyslop. Force measurement techniques in short duration hypersonic facilities. PhD thesis, University of Oxford, 2023.
- [23] Andrew Hyslop, Luke J Doherty, and Matthew McGilvray. Comparison of force measurement techniques in a short duration hypersonic facility. *Experiments in Fluids*, 65(2):21, 2024.
- [24] Liam P McQuellin, Christopher M Kennell, Joni M Sytsma, Rishabh Choudhury, Andrew Neely, David R Buttsworth, and Todd Silvester. Investigating endo-atmospheric separation of a hypersonic flyer-sustainer using wind tunnel based free-flight. In 23rd AIAA International Space Planes and Hypersonic Systems and Technologies Conference, 2020.
- [25] Liam P McQuellin, Andrew Neely, and Gaetano Currao. Considerations for a hypersonic flight test investigating fluid-thermal-structural interactions. In 23rd AIAA International Space Planes and Hypersonic Systems and Technologies Conference, 2020.
- [26] Jack Hillyer, Luke Doherty, Chris Hambidge, and Matthew McGilvray. Extension of test time in ludwieg tunnels. 2022.
- [27] Jack Hillyer, Luke Doherty, Christopher Hambidge, and Matthew McGilvray. Enhancing the test time performance of ludwieg tunnels. In AIAA SCITECH 2024 Forum, page 2754, 2024.
- [28] Matthew McGilvray, Luke J Doherty, Andrew J Neely, Robert Pearce, and Peter Ireland. The oxford high density tunnel. In 20th AIAA International Space Planes and Hypersonic Systems and Technologies Conference, page 3548, 2015.
- [29] McGilvray M Hambidge C Herman T. and Buttsworth D. Total Temperature Measurements In the Oxford High Density Tunnel. *FAR Conference, Monopoli, Italy,* 2019.
- [30] Agung Widodo and David Buttsworth. Stagnation temperature in a cold hypersonic flow produced by a light free piston compression facility. *Experiments in fluids*, 54:1–12, 2013.
- [31] Frederick G Keyes. A summary of viscosity and heat-conduction data for he, a, h2, o2, n2, co, co2, h2o, and air. *Transactions of the American Society of Mechanical Engineers*, 73(5):589–595, 1951.
- [32] Hugh W Coleman and W Glenn Steele. *Experimentation, validation, and uncertainty analysis for engineers*. John Wiley & Sons, 2018.